An optogenetic tool for the activation of endogenous diaphanous-related formins induces thickening of stress fibers without an increase in contractility

Megha Vaman Rao[1], **Pei-Hsuan Chu**[2], **Klaus Michael Hahn**[2,3], and **Ronen Zaidel-Bar**[1,4,*]

[1]Graduate Program in Mechanobiology, Mechanobiology Institute, National University of Singapore, Singapore 117411, Singapore

[2]Department of Pharmacology, University of North Carolina, Chapel Hill, North Carolina 27599, USA

[3]Lineberger Comprehensive Cancer Center, University of North Carolina, Chapel Hill, North Carolina 27599, USA

[4]Department of Bioengineering, National University of Singapore, Singapore 117411, Singapore

Abstract

We have developed an optogenetic technique for the activation of diaphanous related formins. Our approach is based on fusion of the Light-Oxygen-Voltage 2 domain of *Avena sativa* Phototrophin1 to an isolated Diaphanous Autoregulatory Domain from mDia1. This "caged" diaphanous autoregulatory domain was inactive in the dark, but in the presence of blue light rapidly activated endogenous diaphanous related formins. Using an F-actin reporter we observed filopodia and lamellipodia formation as well as a steady increase in F-actin along existing stress fibers, starting within minutes of photo-activation. Interestingly, we did not observe the formation of new stress fibers. Remarkably, a 1.9 fold increase in F-actin was not paralleled by an increase in myosin II along stress fibers and the amount of tension generated by the fibers, as judged by focal adhesion size, appeared unchanged. Our results suggest a decoupling between F-actin accumulation and contractility in stress fibers and demonstrate the utility of photoactivatable diaphanous autoregulatory domain for the study of diaphanous related formin function in cells.

Keywords

Diaphanous related formins; Actin polymerization; stress fiber; Optogenetics; Actomyosin contractility; Light-Oxygen-Voltage domain

Introduction

The actin cytoskeleton organizes the cell interior, maintains its shape, and connects it with its exterior via cell-cell and cell-matrix adhesion sites. Through assembly and disassembly

*Corresponding author: Ronen Zaidel-Bar, Mechanobiology Institute, National University of Singapore, T-lab building #05-01, 5A Engineering Drive 1, Singapore 117411, Tel: +65 6601 1451, Fax: +65 6872 6123, biezbr@nus.edu.sg.

and through association with myosin motors the actin cytoskeleton can change shape and generate forces to facilitate many important cellular processes, such as cell motility, cytokinesis, endocytosis, and wound closure (Pollard and Cooper 2009). The dynamics and architecture of actin networks in the cell are tightly controlled by dozens of actin-binding proteins, which bind monomers and/or filaments of actin and catalyze one or more of the following: filament nucleation, branching, elongation, capping, severing, stabilization, and cross-linking (dos Remedios et al. 2003; Paavilainen et al. 2004; Revenu et al. 2004). Nucleation of actin is an energetically unfavorable step that is overcome by the activity of the Arp2/3 complex, Formins or Spire, each of which, due to its unique features, is responsible for the polymerization of a specialized actin structure. Arp2/3-driven nucleation forms a dendritically branched network (Mullins et al. 1998), which is capable of pushing membranes, such as the leading edge of a migrating cell (Pollard and Borisy 2003). Formins nucleate and promote long unbranched actin filaments (Watanabe and Higashida 2004) that can combine with non-muscle myosin II to form contractile bundles, such as the cytokinetic ring (Tolliday et al. 2002). There are seven sub-families of formins, two of which appear to be neuronal specific and five are widely expressed (Chesarone et al. 2010). Of these, the family of Diaphanous-related formins (DRFs), consisting of mDia1, mDia2 and mDia3, has established roles in lamellipodial and filopodial protrusion (Sarmiento et al. 2008; Schirenbeck et al. 2005), stress fiber formation (Hotulainen and Lappalainen 2006), cell-cell adhesion (Carramusa et al. 2007), cytokinesis (Tolliday et al. 2002; Tominaga et al. 2000), phagocytosis (Brandt et al. 2007), endosomal trafficking (Fernandez-Borja et al. 2005), golgi organization (Zilberman et al. 2011), synaptic growth and stability (Pawson et al. 2008), microtubule stabilization (Palazzo et al. 2001) and transcriptional activation (Tominaga et al. 2000). Structurally, DRFs can be divided into a catalytic C-terminal half, containing the formin homology 1 (FH1), formin homology 2 (FH2), and Diaphanous auto-regulatory domain (DAD) domains, and a regulatory N-terminal half, containing a Rho GTPase-binding domain (RBD), Diaphanous inhibitory domain (DID), dimerization domain (DD), and coiled coil (CC) domain (Higgs 2005). An interaction between the DAD and DID domains keeps the protein locked in a folded state, in which the activity of the FH1 and FH2 is turned off (Li and Higgs 2003). DRFs are turned on by active Rho; binding of Rho-GTP to the RBD of the DRF releases the auto-inhibitory interaction between DAD and DID and frees the FH2 and FH1 domains to bind and polymerize actin (Watanabe et al. 1999).

To date, the study of DRF function in cells has primarily relied on the use of deletion mutants that create constitutively active forms of the DRF, either by deleting the DAD domain or by truncating the N-terminus, leaving only the FH1/FH2 and DAD domains (Watanabe et al. 1999). These constructs have two major caveats, the first being that they involve overexpression of exogenous active DRF at levels that are much higher than endogenous DRF, and secondly, they remove domains that normally interact with other proteins and may regulate the localization of DRF within the cell (Chesarone et al. 2010). Expression of a constitutively active form of RhoA has been used as a means to activate DRFs in cells (Carramusa et al. 2007). This method has the advantage of activating endogenous DRFs, but the obvious drawback is that RhoA has other effectors in the cell, such as Rho-associated protein kinase (ROCK) (Amano et al. 1997; Ishizaki et al. 1997) and PIP5K (Weernink et al. 2004), thus complicating any interpretation of results. Yet another

method to activate endogenous DRFs is the exogenous expression of DAD domains (Alberts 2001; Palazzo et al. 2001; Dong et al. 2003). DAD expression has been shown to induce actin polymerization and SRF activation (Alberts 2001). This method is the cleanest of the three, as it only activates endogenous DRFs and no other pathway. However, it takes from minutes to hours for the DAD protein to accumulate post- injection/transfection and thus the exact timing of DRF activation is not known.

In recent years optogenetic tools have been devised to activate proteins within cells using light (Toettcher et al. 2011). These techniques make use of conformational changes occurring in proteins after light is absorbed. One such protein is the Light-Oxygen-Voltage (LOV) protein from *Avena sativa* Phototropin1 (Christie et al. 1999). Here, we demonstrate that by fusing the LOV domain to the DAD domain of mDia1 we have generated a novel tool that allows photo-activation of endogenous DRF activity in cells. We use this tool to show immediate and sustained actin polymerization all along existing stress fibers (SFs) in serum-starved HeLa cells in response to DRF activation. Furthermore, we found that the 1.9-fold increase in F-actin in SFs was not accompanied by an increase in non-muscle myosin II along the SF and did not change the average size of focal adhesions at the ends of SFs. Thus, our novel tool was able to decouple between F-actin content and contractility in actin stress fibers.

Materials and Methods

Plasmids/DNA Cloning

The cDNA encoding the light, oxygen, and voltage (LOV2-Jα) protein domain of *Avena sativa* (oat) Phototropin1 (404–546) was a gift from Keith Moffat, University of Chicago. Chimeric fusion constructs consisting of LOV2-Jα fused to the DAD domain of mouse Diaphanous-related formin-1 (mDia1) were generated using an overlapping PCR approach, and the fluorescent protein mVenus was inserted, with a short linker (GS_3), at the N terminus of the LOV2-Jα domain to monitor expression and subcellular localization. A short flexible linker (GGS_2) that permits light-induced unfolding of the protein was then inserted between the LOV2-Jα and DAD domains using an overlapping PCR approach. Photo-activatable DAD (PA-DAD) was thus constructed as follows: mVenus-(GS_3)-LOV2-Jα (404–546)–$(GGS)_2$-DAD (1177–1222). The QuickChange (Stratagene) site-directed mutagenesis protocol was used to introduce additional point mutations in the LOV2-Jα domain, including I539E for constitutive activation (lit mutant), and C450M to mimic the dark state of the LOV2-Jα domain. A separate construct with a point mutation in the DAD domain (PA-DAD-M1182A) was also generated using the QuickChange mutagenesis strategy. All the aforementioned constructs were inserted into a pTriEx-4 (Novagen) vector for transient expression in mammalian cells. BFP-tagged PA-DAD was cloned by PCR-amplifying the LOV2-Jα–$(GGS)_2$-DAD cassette and inserting it into pTag-BFP (Evrogen, Russia) using BglII and BamHI sites.

Cloning for the constitutively active full-length mDia1 (CA-mDia1) was performed using the QuickChange site-directed mutagenesis protocol. Mutations V161D and N165D in the GTPase-binding domain and M1182A and L1185A in the DAD domain were introduced

into full-length GFP-tagged mDia1 using primers containing the respective point mutations. The novel plasmids described here will be available through Addgene (www.addgene.org).

Plasmids for alpha-actinin and focal adhesion proteins paxillin, zyxin, and integrin-alpha-V (all tagged with mCherry fluorescent tag) were gifts from Michael Davidson, Florida State University. F-Tractin (comprising amino acids 9–52 of rat ITPKA), an F-actin marker, tagged with tdTomato was a gift from Michael Schell, Uniformed Services University, Bethesda MD (Johnson and Schell 2009). Plasmids encoding myosin regulatory light chain (eGFP-MRLC1) and its phospho-mimetic mutant (pEFGP-MRLC1 T18D, S19D) (Beach et al. 2011) were obtained from Addgene (Tom Egelhoff, Addgene plasmids 35680 and 35682 respectively).

Cell Culture

HeLa (human cervical adenocarcinoma) and NIH3T3 (mouse fibroblasts) were cultured at 37°C and 5% CO_2 atmosphere, in Dulbecco's Modified Eagle Medium (DMEM; Invitrogen) supplemented with 10% FBS (Invitrogen), 2mM L-Glutamine (Invitrogen), and 1% Penicillin-streptomycin (Invitrogen).

Immunofluorescence and Phalloidin staining

Cells for immunofluorescence and/or phalloidin staining were seeded on glass coverslips, followed by transfection with the desired plasmids using Lipofectamine 2000 (Invitrogen) as per manufacturer's instructions. Samples were processed for immunostaining 22–24hr post-transfection. Briefly, cells were fixed for 15 minutes in warm 4% paraformaldehyde followed by permeabilization with 0.25% Triton X-100 for 3 minutes. Samples were then stained at room temperature with the appropriate dilution of desired primary antibody for one hour, followed by secondary antibody and/or Tritc-conjugated Phalloidin (Sigma-Aldrich) for 30min in dark conditions before mounting them on glass slides using FlourSave mounting media (Merck Millipore). Primary antibodies used were mouse anti-paxillin (BD Transduction Laboratories) and rabbit anti-myosin IIA (Sigma-Aldrich). Secondary antibodies were donkey anti-mouse or anti-rabbit, conjugated to Alexa 568 or Alexa 647 (Invitrogen).

Transfection

Cells for live imaging were seeded on 30mm glass coverslips in DMEM medium supplemented with 10% FBS at a density of $2x10^5$ cells/ml in a 35mm dish. Typically 0.3µg of mVenus-LOV-wt-6aa-DAD and 0.2µg of F-Tractin-tdTomato or 0.3µg of MRLC plasmids or a focal adhesion marker was used for transient transfection with Lipofectamine 2000. Following transfection, cells were serum-starved for ~16hr prior to imaging. Sample preparation and handling was performed in the dark or under red light, due to the light sensitivity of the LOV domain. Care was taken to avoid exposure of transfected cells to ambient light and wavelengths <500nm immediately before imaging experiments.

Live-cell imaging and formin inhibition

Live-cell imaging was carried out at 37°C and 5% CO_2 atmosphere in a heated chamber in DMEM without serum and phenol red, supplemented with 25mM HEPES (Invitrogen).

Images were acquired using a microscope (Model Ti, Nikon) equipped with a Spinning-Disk confocal head (Model CSU-X1, Yokogawa Corporation), Laser launch unit (iLas2, Roper Scientific) and a CCD camera (Evolve Rapid-Cal, Photometrics). A 60X Plan-Apo 1.40NA objective (Nikon) was used for image acquisition and z-axis movement was controlled by the Perfect Focus System on the microscope (Nikon). MetaMorph software (Molecular Devices) was used for image acquisition. Activation of PA-DAD or PA-DAD-M1182A was carried out using an illumination regime of 500ms exposure with a 405nm laser at intervals of 3 minutes. Actin and focal adhesion markers were imaged using a 561nm laser at 30-second time intervals. For experiments involving treatment with the small molecule inhibitor of FH2 domains (SMIFH2; ChemBridge Corp. San-Diego, USA), sample preparation was the same as described earlier. Prior to imaging, samples were incubated with SMIFH2 (30µm, prepared in DMSO) for 3hr and imaged using a similar activation regime as described above, in presence of the drug.

Image analysis

Quantification of fluorescent intensity was performed using standard ImageJ measurement tools (NIH, USA). Phalloidin or F-Tractin intensity was measured in manually drawn polygons surrounding either whole cells, individual SFs, segments of SFs or regions inside the cell devoid of SFs. To quantify FAs, we used the "subtract background" and "thresholding" functions to create a binary image identifying all FAs in each frame of a movie. The "analyze particles" function was then applied to calculate size, number and intensity of each FA. Data were regularly registered using Microsoft Excel 2011 and statistical analysis and graphs were drawn in Prism 6 software (GraphPad Software, Inc.). Quantitative datasets were subjected to Student's t-test using the statistical functions available in Prism 6. Images were prepared for publication using Adobe Photoshop CS6 v13.0.1x64 (Adobe Systems, San Jose, CA).

Results

Constructing PA-DAD

We sought to generate a tool to activate endogenous DRFs, in particular members of the Diaphanous family (collectively referred to hereafter as Dia), in a temporally controlled manner. Dia is held inactive by an intra-molecular interaction between the N-terminal Diaphanous inhibitory domain (DID) and C-terminal Diaphanous auto-regulatory domain (DAD) (Li and Higgs 2003). Alberts had shown that it is possible to activate endogenous mDia by expressing an exogenous DAD domain, which competes with the endogenous DAD for binding of the DID domain and thus releases the auto-inhibition (Alberts 2001). Previously, we have used the photo-switchable LOV domain of *Avena sativa* Phototropin1 to make a Photo-activatable Rac1 (PA-Rac) (Wu et al. 2009). Here, we fused the complete LOV2-Jα sequence (404–546) to the N-terminus of mDia1 DAD (1177–1222), anticipating that the LOV domain in its closed conformation would block the binding of the DAD with endogenous Dia, and that light-induced unwinding of the Jα helix would release steric inhibition, leading to Dia activation (Figure 1A). We used F-actin polymerization in HeLa cells, quantified by phalloidin fluorescence intensity, as a measure of Dia activation. As a positive control we used a GFP-tagged constitutively active full length mDia1 (GFP-CA-

mDia1) that we generated by mutating the C-terminal DAD domain (M1182A and L1185A) so that it cannot interact with the DID domain (Gould et al. 2011) and the N-terminal Rho-GTPase binding domain (V161D and N165D) (Otomo et al. 2005; Rose et al. 2005) so that it does not sequester active RhoA (Figure 1B). Expression of CA-mDia1 led to a 1.49 (±0.02, n=30 cells)-fold increase in phalloidin staining relative to non-transfected control cells (Figure 1C). Expression of the mDia1 DAD domain fused to mVenus on its N-terminus led to a 1.6 (±0.05, n=30)-fold increase in phalloidin staining (Figure 1C). However, the fusion of either light or dark conformation mutants of the LOV2 domain to the N-terminus of DAD completely inhibited its effect on endogenous Dia, as evident by the lack of increase in F-actin accumulation in these cells (Figure 1C). To circumvent this problem we inserted linkers of varying lengths between the LOV2 and DAD domains. We found that a six amino acid linker was the optimal length, exhibiting a 1.43 (±0.02, n=30)-fold increase in phalloidin staining with the LOV2 in the open conformation (lit mutant) and only a modest increase (1.19±0.05-fold) with the LOV2 in the closed conformation (dark mutant) (Figure 1C). From here on we refer to the wild-type LOV2 fused to the DAD from mDia1 with a six amino acid linker as Photo-activatable DAD (PA-DAD).

Effects of PA-DAD activation on the actin cytoskeleton

To observe the effects of endogenous Dia activation on actin polymerization in real time, we expressed mVenus-tagged PA-DAD in HeLa cells along with the F-actin reporter F-Tractin-tdTomato. Cells were serum-starved after transfection to reduce the overall level of Rho activity in them. Without photo-activation, cells expressing PA-DAD showed a slight increase in the number of SFs and filopodial protrusions compared to non-transfected controls, indicating some degree of "leakiness" of the PA-DAD. However, in the absence of photo-activation, and imaging only F-Tractin-tdTomato in these cells using a 561nm laser we did not detect a noticeable change in F-Tractin levels or in cell morphology over a one-hour period (Figure 2A). By contrast, photo-activating PA-DAD with a 405nm laser resulted in a steady increase in F-actin content of SFs, resulting, on average, in a 1.9-fold increase in F-Tractin fluorescent intensity and/or an increase in SF width (Figure 2A and 2B). This increase in actin polymerization was evidently formin-dependent since activation of PA-DAD in the presence of a small molecule inhibitor of FH2 domains (SMIFH2; Rizvi et al. 2009) did not result in increased actin polymerization (Figure 2A). Furthermore, a point mutation (M1182A) in the DAD domain shown to disrupt its interaction with mDia DID domain, but not to affect its G-actin binding ability (Gould et al. 2011), substantially abrogated the capacity of PA-DAD-M1182A to induce actin polymerization upon photoactivation (Figure 2A). Measuring the fluorescence intensity of the mVenus protein fused to PA-DAD we found a positive correlation between the expression level of PA-DAD and the degree of increase in actin polymerization reported by F-Tractin (Figure 2C).

In addition to thickening of stress fibers we observed a doubling in the number of filopodia forming throughout the cell periphery (Figure 3A and 3B) and bursts of actin polymerization throughout the cell body, appearing as clouds or "worms", resulting in a 1.5-fold increase in the level of F-actin in the cell body (Figure 3C and 3D). To verify that F-Tractin is faithfully reporting on a *bona-fide* increase in F-actin we co-transfected PA-DAD cells with fluorescently tagged alpha-actinin, an F-actin binding protein and a component of SFs.

Following photo-activation mCherry-alpha-actinin showed an increase in intensity along SFs that resembled the increase observed with F-Tractin (Supplementary Figure 1). Similar effects of PA-DAD activation were also obtained in NIH3T3 fibroblasts, except that in addition to filopodia formation, multiple lamellipodial protrusions were observed after PA-DAD activation (Supplementary Figure 2).

We attempted to locally activate Dia by restricting the 405nm illumination to a small region within the cell. However, despite the local illumination we observed an increase in F-actin throughout the cell just as in whole field illumination indicating that the activated PA-DAD diffused away from the illumination spot faster than its switching to the dark conformation.

Dia activity along SF

Current models of SF assembly postulate that SFs either form by the coming together of pre-assembled bundles of F-actin and myosin (Cramer et al. 1997; Hirata et al. 2007; Machesky and Hall 1997; Verkhovsky et al. 1995), or by actin polymerization at the ends of SFs, where they connect with focal adhesions (Endlich et al. 2007; Hotulainen and Lappalainen 2006; Noria et al. 2004; Okabe and Hirokawa 1989). If actin polymerization only occurs at the ends of SFs, we reasoned, we should first see an increase in F-Tractin intensity at the ends of SFs, followed by an increase in intensity at the central region of the SF at a later time. To test this idea we segmented individual SFs into three equal parts and followed the changes over time in total fluorescent intensity for each segment. We found that in most cases the increase in F-Tractin intensity occurred concurrently in the three segments. In some cases the three segments appeared to change independently of each other and we could observe an increase in the central region before an increase at the ends of the SF (Figure 4A). Thus, our observations are consistent with actin polymerization occurring all along the SF and not restricted to either end.

HeLa cells typically assemble two types of SFs: Central SF and Peripheral SF. It has previously been shown that peripheral SFs are more dependent on Myosin light chain kinase (MLCK) whereas central SFs are more dependent on Rho-associated protein kinase (ROCK) (Katoh et al. 2001). In line with this distinction, after 16–18 hours of serum starvation (a condition of low Rho/ROCK activity) we found that HeLa cells had lost most of their central SFs while retaining their peripheral SFs. Noting the difference in regulation of peripheral versus central SFs we wondered whether Dia activation will differentially affect these two types of SFs. To test this idea we quantified the change in F-Tractin intensity after photo-activation in individual SFs from either the center or periphery of cells. As shown in Figure 4B, while the level of F-actin in both types of SF increased in response to PA-DAD activation, the level of F-actin in peripheral SF rose faster and reached a higher level as compared with central SF.

Interestingly, while PA-DAD activation led to substantial actin polymerization within existing SFs we did not observe a single instance of de-novo assembly of a SF. As mentioned earlier, due to serum starvation some cells had few central SF and some had no central SF at all. In the cells with few SF, upon photo-activation of PA-DAD some SF grew longer, others branched or diverged to create in the end more SF than at the beginning, but cells that had no central SF at the beginning failed to polymerize SF till the end of our

acquisition (Figure 4C). In conditions of no activation, the existing central SFs did not show any change during the course of imaging.

Dia activation and focal adhesions

The majority of SFs in HeLa cells are ventral SF, which are anchored at focal adhesions (FAs) on both ends (Small et al. 1998). It is well established that FAs depend on the actomyosin contractility created by the SF for their assembly, growth and maintenance (Balaban et al. 2001; Chrzanowska-Wodnicka and Burridge 1996; Oakes et al. 2012). In fact, thanks to their tensile connection to SFs, FAs function as mechanosensors and rapidly respond to increases/decreases in tension by assembly/disassembly (Bershadsky et al. 2006; Riveline et al. 2001). Therefore, we wondered whether the 1.9-fold increase in F-actin in SFs following Dia activation is accompanied by a corresponding growth of FA. To test this we co-expressed PA-DAD with several known markers of FAs, namely paxillin, zyxin, and integrin-alpha-V. Surprisingly, following activation of PA-DAD we did not observe any significant change in the number, size, shape or intensity of FA visualized by these markers (Figure 5A and 5B and data not shown).

Dia activation and contractility

The fact that FAs did not grow in response to PA-DAD activation can be taken as an indication that the growth in SF F-actin density and thickness was not accompanied by an increase in contractility. This could be because myosin is not being recruited into the new F-actin structures or because myosin is not being activated. To distinguish between these possibilities we co-expressed PA-DAD with Myosin Regulatory Light Chain-GFP (MRLC-GFP) or a phospho-mimetic mutant version (T18D, S19D) of MRLC, pMRLC-GFP, along with FA markers (mCherry-integrin-alpha-V or mCherry-paxillin). Under the same photo-activation conditions in which we observed ~90% increase in F-Tractin intensity in SF we only detect a mild (14%) increase in MRLC recruitment into SF (Figure 6A), indicating that myosin is not being substantially recruited into the new F-actin structures. In line with this observation, expression of the phospho-mimetic MRLC, which is presumably constitutively active (Beach et al. 2011), does not lead to any increase in FA size or intensity (Figure 6B and 6C). Thus, it appears that actomyosin contractility along the SF does not increase despite the increase in actin filaments due to the lack of myosin recruitment.

The notion that Dia activation can lead to a substantial increase in F-actin in SF without a corresponding increase in focal adhesions is supported by the results of long-term expression of CA-mDia1. Compared to control eGFP-transfected cells, GFP-CA-mDia1 cells have 50% more F-actin organized in SF (Figure 1C), but the level of organized myosin in the cell is only 22% higher than the control (Supplementary Figure 3A) and the number, size and intensity of FA is not significantly different than the control (Supplementary Figures 3B and 3C).

Discussion

We have devised a means to activate endogenous diaphanous related formins in live cells using light. Our optogenetic tool takes advantage of the natural capability of the Dia DAD

domain to bind Dia DID domain. This intra-molecular interaction maintains Dia in a folded, inactive state, but exogenous DAD competes with the intra-molecular DAD for binding to the DID and thereby releases the inhibition. The DAD domain has been previously used to activate endogenous mDia (Alberts 2001; Palazzo et al. 2001, Dong et al. 2003). Our contribution is to add precise temporal control by "caging" the DAD using an LOV domain so that it can be "uncaged" on demand by illumination with blue light. By monitoring F-actin polymerization in cells using F-Tractin we were able, within minutes, to detect the effects of photo-activating PA-DAD. Alberts has shown that the effects of DAD on actin polymerization and SRF are dependent on endogenous mDia, as they were blocked by co-injection of anti mDia antibodies (Alberts 2001). We further verified the efficacy and specificity of PA-DAD by showing that it looses its activity in the presence of the formin inhibitor SMIFH2 or with a mutation in the DAD that interferes with its binding to mDia's DID domain. Although our tool is based on the DAD domain of mouse mDia1, based on sequence homology it will most likely activate all three DRF. In order to attribute the effect on actin polymerization we observed in cells to a particular Dia isoform, one would have to combine photo-activation with knockdown of the other two Dia isoforms or work in cells that do not express them all. We were unable to use PA-DAD to activate Dia in a spatially confined region within a cell. This could be due to rapid diffusion of the activated PA-DAD or the diffusion of the activated PA-DAD-Dia complex or both.

PA-DAD offers significant advantages over existing tools for the study of DRF function in cells. To date, most of our knowledge on DRFs stems from studies involving overexpression of a constitutively active deletion mutant of Dia, observed many hours after transfection. Using PA-DAD we were able, for the first time, to follow in real-time the cellular response following activation of endogenous Dia in its native localization within the cell.

Dia activity has established effects on microtubules (Gaillard et al. 2011; Palazzo et al. 2001) and transcription (Copeland and Treisman 2002), but in this study, as proof of principle, we focused our attention on the effects of Dia on actin polymerization. We observed Dia-induced actin polymerization all over the cell, but in particular we noted a robust induction of filopodia and robust thickening of existing stress fibers. The appearance of filopodia is consistent with previous reports showing overexpression of the active form of mDia2 will produce ectopic filopodia (Block et al. 2008; Schirenbeck et al. 2005). Our observation of actin polymerization along stress fibers is novel. DRFs have been proposed to play a role in polymerization of actin at the ends of dorsal SF, in close proximity to focal adhesions (Hotulainen and Lappalainen 2006), but they haven't, to the best of our knowledge, been implicated in actin polymerization along the length of the SF, where we clearly observe increases in F-actin content upon PA-DAD activation. While the simplest explanation for our observation is that Dia localizes to the plus ends of actin filaments all along the SF, we cannot rule out the possibility that actin filaments were first polymerized in the cytoplasm and then incorporated into the SF.

Interestingly, while we observed thickening and elongation, as well as branching and splitting of SF, we did not observe any *de novo* appearance of SF, indicating that factors other than DRFs are necessary for their formation. Furthermore, while the F-actin content of SFs increased by 1.9-fold we did not observe an equivalent change in the level of non-

muscle myosin II in SF, suggesting that the creation of F-actin bundles by themselves is not sufficient for myosin recruitment and that other factors are needed. Since RhoA activation results in thicker SFs and increased myosin contractility (Chrzanowska-Wodnicka and Burridge 1996; Ridley and Hall 1992), as indicated by the size of FA, it is possible that ROCK activation is responsible not only for activation of myosin, but also for its recruitment into SF, as has been shown for the cytokinetic furrow (Kosako et al. 2000).

In summary, we demonstrated that PA-DAD provides a powerful new approach to probe DRF function in live cells, using conventional microscopy techniques, and shed new light on the involvement of DRFs in SF maintenance.

Supplementary Material

Refer to Web version on PubMed Central for supplementary material.

Acknowledgments

References

Alberts AS. Identification of a carboxyl-terminal diaphanous-related formin homology protein autoregulatory domain. J Biol Chem. 2001; 276(4):2824–2830. [PubMed: 11035012]

Amano M, Chihara K, Kimura K, Fukata Y, Nakamura N, Matsuura Y, Kaibuchi K. Formation of actin stress fibers and focal adhesions enhanced by Rho-kinase. Science. 1997; 275(5304):1308–1311. [PubMed: 9036856]

Balaban NQ, Schwarz US, Riveline D, Goichberg P, Tzur G, Sabanay I, Mahalu D, Safran S, Bershadsky A, Addadi L, et al. Force and focal adhesion assembly: a close relationship studied using elastic micropatterned substrates. Nat Cell Biol. 2001; 3(5):466–472. [PubMed: 11331874]

Beach JR, Licate LS, Crish JF, Egelhoff TT. Analysis of the role of Ser1/Ser2/Thr9 phosphorylation on myosin II assembly and function in live cells. BMC Cell Biol. 2011; 12:52. [PubMed: 22136066]

Bershadsky AD, Ballestrem C, Carramusa L, Zilberman Y, Gilquin B, Khochbin S, Alexandrova AY, Verkhovsky AB, Shemesh T, Kozlov MM. Assembly and mechanosensory function of focal adhesions: experiments and models. Eur J Cell Biol. 2006; 85(3–4):165–173. [PubMed: 16360240]

Block J, Stradal TE, Hanisch J, Geffers R, Kostler SA, Urban E, Small JV, Rottner K, Faix J. Filopodia formation induced by active mDia2/Drf3. J Microsc. 2008; 231(3):506–517. [PubMed: 18755006]

Brandt DT, Marion S, Griffiths G, Watanabe T, Kaibuchi K, Grosse R. Dia1 and IQGAP1 interact in cell migration and phagocytic cup formation. J Cell Biol. 2007; 178(2):193–200. [PubMed: 17620407]

Carramusa L, Ballestrem C, Zilberman Y, Bershadsky AD. Mammalian diaphanous-related formin Dia1 controls the organization of E-cadherin-mediated cell-cell junctions. J Cell Sci. 2007; 120(Pt 21):3870–3882. [PubMed: 17940061]

Chesarone MA, DuPage AG, Goode BL. Unleashing formins to remodel the actin and microtubule cytoskeletons. Nat Rev Mol Cell Biol. 2010; 11(1):62–74. [PubMed: 19997130]

Christie JM, Salomon M, Nozue K, Wada M, Briggs WR. LOV (light, oxygen, or voltage) domains of the blue-light photoreceptor phototropin (nph1): binding sites for the chromophore flavin mononucleotide. Proc Natl Acad Sci U S A. 1999; 96(15):8779–8783. [PubMed: 10411952]

Chrzanowska-Wodnicka M, Burridge K. Rho-stimulated contractility drives the formation of stress fibers and focal adhesions. J Cell Biol. 1996; 133(6):1403–1415. [PubMed: 8682874]

Copeland JW, Treisman R. The diaphanous-related formin mDia1 controls serum response factor activity through its effects on actin polymerization. Mol Biol Cell. 2002; 13(11):4088–4099. [PubMed: 12429848]

Cramer LP, Siebert M, Mitchison TJ. Identification of novel graded polarity actin filament bundles in locomoting heart fibroblasts: implications for the generation of motile force. J Cell Biol. 1997; 136(6):1287–1305. [PubMed: 9087444]

Dong Y, Pruyne D, Bretscher A. Formin-dependent actin assembly is regulated by distinct modes of Rho signaling in yeast. J Cell Biol. 2003; 161(6):1081–1092. [PubMed: 12810699]

dos Remedios CG, Chhabra D, Kekic M, Dedova IV, Tsubakihara M, Berry DA, Nosworthy NJ. Actin binding proteins: regulation of cytoskeletal microfilaments. Physiol Rev. 2003; 83(2):433–473. [PubMed: 12663865]

Endlich N, Otey CA, Kriz W, Endlich K. Movement of stress fibers away from focal adhesions identifies focal adhesions as sites of stress fiber assembly in stationary cells. Cell Motil Cytoskeleton. 2007; 64(12):966–976. [PubMed: 17868136]

Fernandez-Borja M, Janssen L, Verwoerd D, Hordijk P, Neefjes J. RhoB regulates endosome transport by promoting actin assembly on endosomal membranes through Dia1. J Cell Sci. 2005; 118(Pt 12):2661–2670. [PubMed: 15944396]

Gaillard J, Ramabhadran V, Neumanne E, Gurel P, Blanchoin L, Vantard M, Higgs HN. Differential interactions of the formins INF2, mDia1, and mDia2 with microtubules. Mol Biol Cell. 2011; 22(23):4575–4587. [PubMed: 21998204]

Gould CJ, Maiti S, Michelot A, Graziano BR, Blanchoin L, Goode BL. The formin DAD domain plays dual roles in autoinhibition and actin nucleation. Curr Biol. 2011; 21(5):384–390. [PubMed: 21333540]

Higgs HN. Formin proteins: a domain-based approach. Trends Biochem Sci. 2005; 30(6):342–353. [PubMed: 15950879]

Hirata H, Tatsumi H, Sokabe M. Dynamics of actin filaments during tension-dependent formation of actin bundles. Biochim Biophys Acta. 2007; 1770(8):1115–1127. [PubMed: 17498881]

Hotulainen P, Lappalainen P. Stress fibers are generated by two distinct actin assembly mechanisms in motile cells. J Cell Biol. 2006; 173(3):383–394. [PubMed: 16651381]

Ishizaki T, Naito M, Fujisawa K, Maekawa M, Watanabe N, Saito Y, Narumiya S. p160ROCK, a Rho-associated coiled-coil forming protein kinase, works downstream of Rho and induces focal adhesions. FEBS Lett. 1997; 404(2–3):118–124. [PubMed: 9119047]

Johnson HW, Schell MJ. Neuronal IP3 3-kinase is an F-actin-bundling protein: role in dendritic targeting and regulation of spine morphology. Mol Biol Cell. 2009; 20(24):5166–5180. [PubMed: 19846664]

Katoh K, Kano Y, Amano M, Kaibuchi K, Fujiwara K. Stress fiber organization regulated by MLCK and Rho-kinase in cultured human fibroblasts. Am J Physiol Cell Physiol. 2001; 280(6):C1669–C1679. [PubMed: 11350763]

Kosako H, Yoshida T, Matsumura F, Ishizaki T, Narumiya S, Inagaki M. Rho-kinase/ROCK is involved in cytokinesis through the phosphorylation of myosin light chain and not ezrin/radixin/moesin proteins at the cleavage furrow. Oncogene. 2000; 19(52):6059–6064. [PubMed: 11146558]

Li F, Higgs HN. The mouse Formin mDia1 is a potent actin nucleation factor regulated by autoinhibition. Curr Biol. 2003; 13(15):1335–1340. [PubMed: 12906795]

Machesky LM, Hall A. Role of actin polymerization and adhesion to extracellular matrix in Rac- and Rho-induced cytoskeletal reorganization. J Cell Biol. 1997; 138(4):913–926. [PubMed: 9265656]

Mullins RD, Heuser JA, Pollard TD. The interaction of Arp2/3 complex with actin: nucleation, high affinity pointed end capping, and formation of branching networks of filaments. Proc Natl Acad Sci U S A. 1998; 95(11):6181–6186. [PubMed: 9600938]

Noria S, Xu F, McCue S, Jones M, Gotlieb AI, Langille BL. Assembly and reorientation of stress fibers drives morphological changes to endothelial cells exposed to shear stress. Am J Pathol. 2004; 164(4):1211–1223. [PubMed: 15039210]

Oakes PW, Beckham Y, Stricker J, Gardel ML. Tension is required but not sufficient for focal adhesion maturation without a stress fiber template. J Cell Biol. 2012; 196(3):363–374. [PubMed: 22291038]

Okabe S, Hirokawa N. Incorporation and turnover of biotin-labeled actin microinjected into fibroblastic cells: an immunoelectron microscopic study. J Cell Biol. 1989; 109(4 Pt 1):1581–1595. [PubMed: 2677022]

Otomo T, Otomo C, Tomchick DR, Machius M, Rosen MK. Structural basis of Rho GTPase-mediated activation of the formin mDia1. Mol Cell. 2005; 18(3):273–281. [PubMed: 15866170]

Paavilainen VO, Bertling E, Falck S, Lappalainen P. Regulation of cytoskeletal dynamics by actin-monomer-binding proteins. Trends Cell Biol. 2004; 14(7):386–394. [PubMed: 15246432]

Palazzo AF, Cook TA, Alberts AS, Gundersen GG. mDia mediates Rho-regulated formation and orientation of stable microtubules. Nat Cell Biol. 2001; 3(8):723–729. [PubMed: 11483957]

Pawson C, Eaton BA, Davis GW. Formin-dependent synaptic growth: evidence that Dlar signals via Diaphanous to modulate synaptic actin and dynamic pioneer microtubules. J Neurosci. 2008; 28(44):11111–11123. [PubMed: 18971454]

Pollard TD, Borisy GG. Cellular motility driven by assembly and disassembly of actin filaments. Cell. 2003; 112(4):453–465. [PubMed: 12600310]

Pollard TD, Cooper JA. Actin, a central player in cell shape and movement. Science. 2009; 326(5957): 1208–1212. [PubMed: 19965462]

Revenu C, Athman R, Robine S, Louvard D. The co-workers of actin filaments: from cell structures to signals. Nat Rev Mol Cell Biol. 2004; 5(8):635–646. [PubMed: 15366707]

Ridley AJ, Hall A. The small GTP-binding protein rho regulates the assembly of focal adhesions and actin stress fibers in response to growth factors. Cell. 1992; 70(3):389–399. [PubMed: 1643657]

Riveline D, Zamir E, Balaban NQ, Schwarz US, Ishizaki T, Narumiya S, Kam Z, Geiger B, Bershadsky AD. Focal contacts as mechanosensors: externally applied local mechanical force induces growth of focal contacts by an mDia1-dependent and ROCK-independent mechanism. J Cell Biol. 2001; 153(6):1175–1186. [PubMed: 11402062]

Rizvi SA, Neidt EM, Cui J, Feiger Z, Skau CT, Gardel ML, Kozmin SA, Kovar DR. Identification and characterization of a small molecule inhibitor of formin-mediated actin assembly. Chem Biol. 2009; 16(11):1158–1168. [PubMed: 19942139]

Rose R, Weyand M, Lammers M, Ishizaki T, Ahmadian MR, Wittinghofer A. Structural and mechanistic insights into the interaction between Rho and mammalian Dia. Nature. 2005; 435(7041):513–518. [PubMed: 15864301]

Sarmiento C, Wang W, Dovas A, Yamaguchi H, Sidani M, El-Sibai M, Desmarais V, Holman HA, Kitchen S, Backer JM, et al. WASP family members and formin proteins coordinate regulation of cell protrusions in carcinoma cells. J Cell Biol. 2008; 180(6):1245–1260. [PubMed: 18362183]

Schirenbeck A, Bretschneider T, Arasada R, Schleicher M, Faix J. The Diaphanous-related formin dDia2 is required for the formation and maintenance of filopodia. Nat Cell Biol. 2005; 7(6):619–625. [PubMed: 15908944]

Small JV, Rottner K, Kaverina I, Anderson KI. Assembling an actin cytoskeleton for cell attachment and movement. Biochim Biophys Acta. 1998; 1404(3):271–281. [PubMed: 9739149]

Toettcher JE, Voigt CA, Weiner OD, Lim WA. The promise of optogenetics in cell biology: interrogating molecular circuits in space and time. Nat Methods. 2011; 8(1):35–38. [PubMed: 21191370]

Tolliday N, VerPlank L, Li R. Rho1 directs formin-mediated actin ring assembly during budding yeast cytokinesis. Curr Biol. 2002; 12(21):1864–1870. [PubMed: 12419188]

Tominaga T, Sahai E, Chardin P, McCormick F, Courtneidge SA, Alberts AS. Diaphanous-related formins bridge Rho GTPase and Src tyrosine kinase signaling. Mol Cell. 2000; 5(1):13–25. [PubMed: 10678165]

Verkhovsky AB, Svitkina TM, Borisy GG. Myosin II filament assemblies in the active lamella of fibroblasts: their morphogenesis and role in the formation of actin filament bundles. J Cell Biol. 1995; 131(4):989–1002. [PubMed: 7490299]

Watanabe N, Higashida C. Formins: processive cappers of growing actin filaments. Exp Cell Res. 2004; 301(1):16–22. [PubMed: 15501440]

Watanabe N, Kato T, Fujita A, Ishizaki T, Narumiya S. Cooperation between mDia1 and ROCK in Rho-induced actin reorganization. Nat Cell Biol. 1999; 1(3):136–143. [PubMed: 10559899]

Weernink PA, Meletiadis K, Hommeltenberg S, Hinz M, Ishihara H, Schmidt M, Jakobs KH. Activation of type I phosphatidylinositol 4-phosphate 5-kinase isoforms by the Rho GTPases, RhoA, Rac1, and Cdc42. J Biol Chem. 2004; 279(9):7840–7949. [PubMed: 14681219]

Wu YI, Frey D, Lungu OI, Jaehrig A, Schlichting I, Kuhlman B, Hahn KM. A genetically encoded photoactivatable Rac controls the motility of living cells. Nature. 2009; 461(7260):104–108. [PubMed: 19693014]

Zilberman Y, Alieva NO, Miserey-Lenkei S, Lichtenstein A, Kam Z, Sabanay H, Bershadsky A. Involvement of the Rho-mDia1 pathway in the regulation of Golgi complex architecture and dynamics. Mol Biol Cell. 2011; 22(16):2900–2911. [PubMed: 21680709]
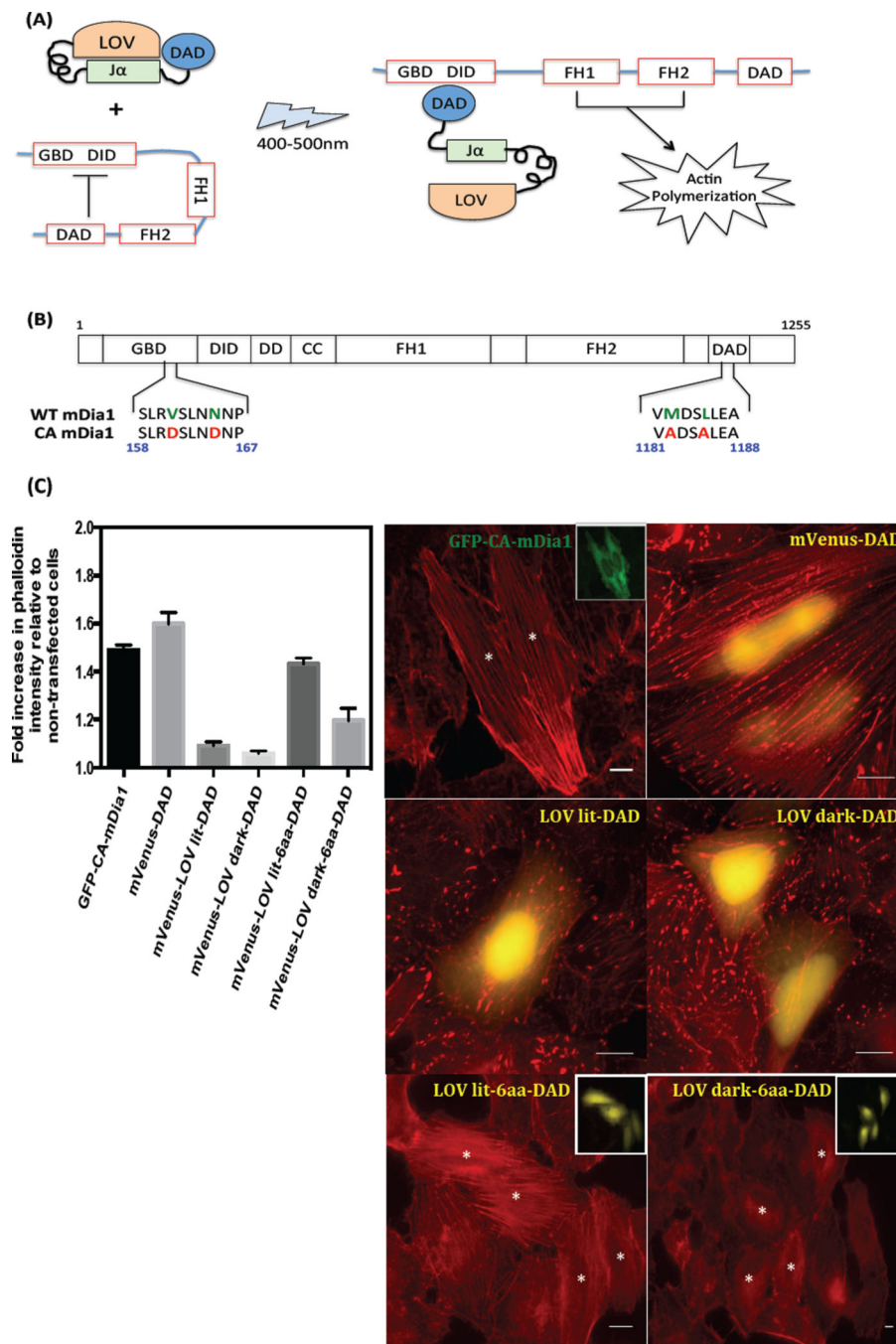
Figure 1. Construction and characterization of photoactivatable-DAD

(**A**) Cartoon representation of photo-activatable (PA-DAD) design. Exogenous, photo-activatable DAD is used to activate endogenous DRFs by releasing the intra-molecular auto-inhibition of DRFs, upon stimulation with blue light (**B**) Mutations introduced into the GTPase-binding domain (GBD) and Diaphanous Autoregulatory Domain (DAD) of full-length wild-type mDia1 to construct constitutively active-mDia1 (CA-mDia1) (**C**) Quantification and representative images of HeLa cells transfected with GFP-CA-mDia1, mVenus-DAD, mVenus-tagged LOV-DAD fusion constructs with the LOV in lit (open) and

dark (closed) conformations, and with the insertion of a 6aa linker (transfected cells marked with asterisks). Cells were stained with TRITC-conjugated phalloidin to visualize actin. GFP-CA-mDia1 and mVenus-DAD were used as positive controls to demonstrate activation of endogenous Dia and production of stress fibers. Average intensity of phalloidin staining in cell body was measured for 30 cells from two separate experiments in each case. Error bars represent s.e.m. Bar, 10μm.
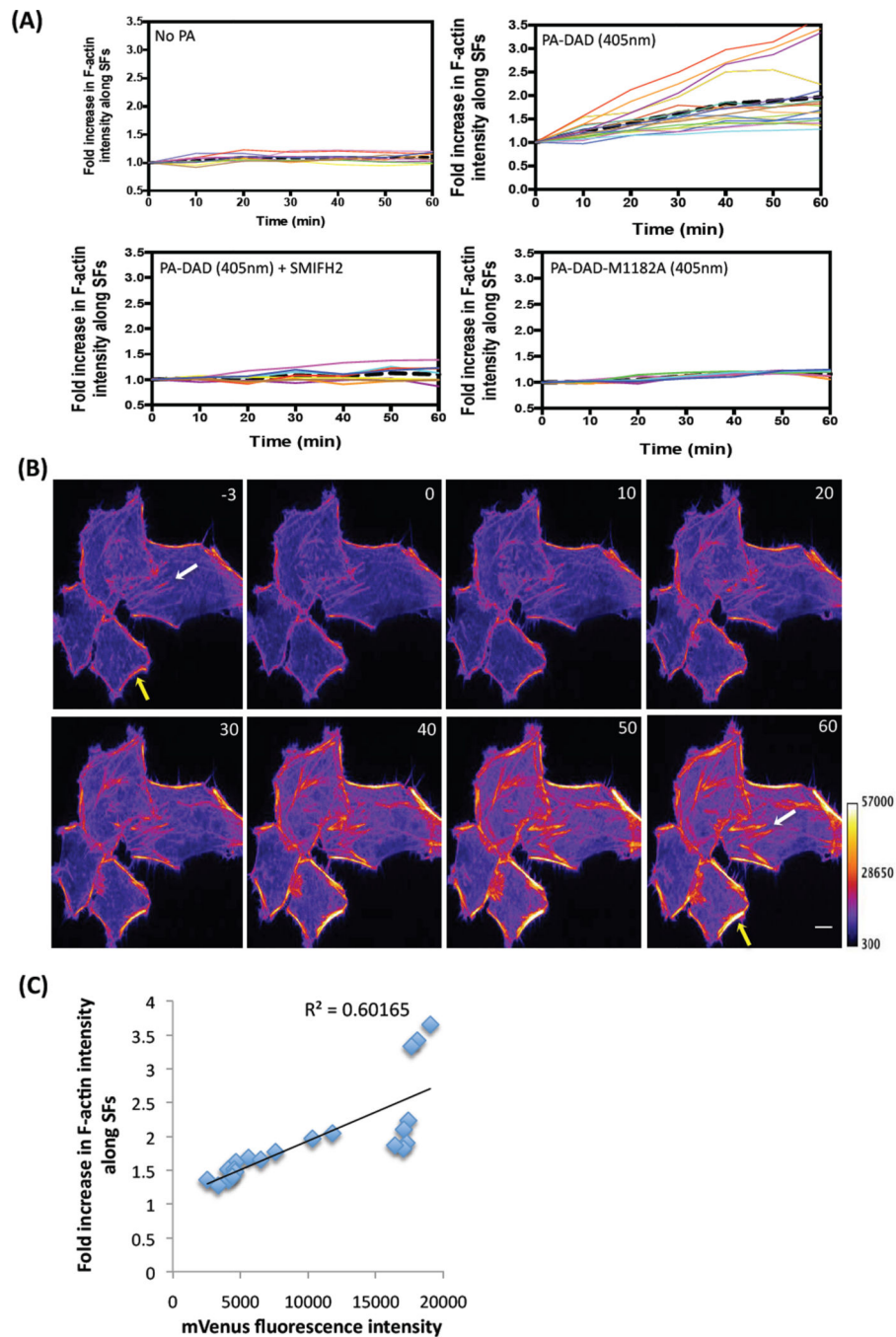
Figure 2. Effects of PA-DAD activation on the actin cytoskeleton of HeLa cells
HeLa cells transfected with mVenus-PA-DAD and the F-actin reporter F-Tractin-tdTomato
were subjected to periodic photo-activation with a 405nm laser at intervals of 3 minutes **(A)**
Quantification of increase in F-Tractin intensity at peripheral SFs during repeated photo-
activation (PA). Change in intensity of individual SFs was followed by drawing polygons
around them. Each colored line in the graph represents an individual SF while the black
broken line indicates the average increase in intensity of several SFs analyzed (n=11 SFs for
No PA, 21 SFs for PA at 405nm). Inhibition of endogenous formins using the small

molecule inhibitor of formin activity, SMIFH2, abolishes the ability of PA-DAD to stimulate actin polymerization (n=9 SFs). Mutation M1182A introduced into the DAD domain of PA-DAD does not induce actin polymerization upon photo-activation (n=9 SFs). **(B)** Images taken from a time-lapse movie of HeLa cells transfected with mVenus-PA-DAD and F-Tractin-tdTomato. Photo-activation of PA-DAD leads to a steady increase in the intensity of both peripheral SFs (representative example marked with yellow arrow at time -3 and 60) and central SFs (white arrow in -3 and 60). Time shown in minutes. Bar, 10μm. **(C)** Correlation between the level of PA-DAD expression, as measured by mVenus fluorescence intensity, and the increase in F-actin along stress fibers, as measured by F-Tractin intensity.
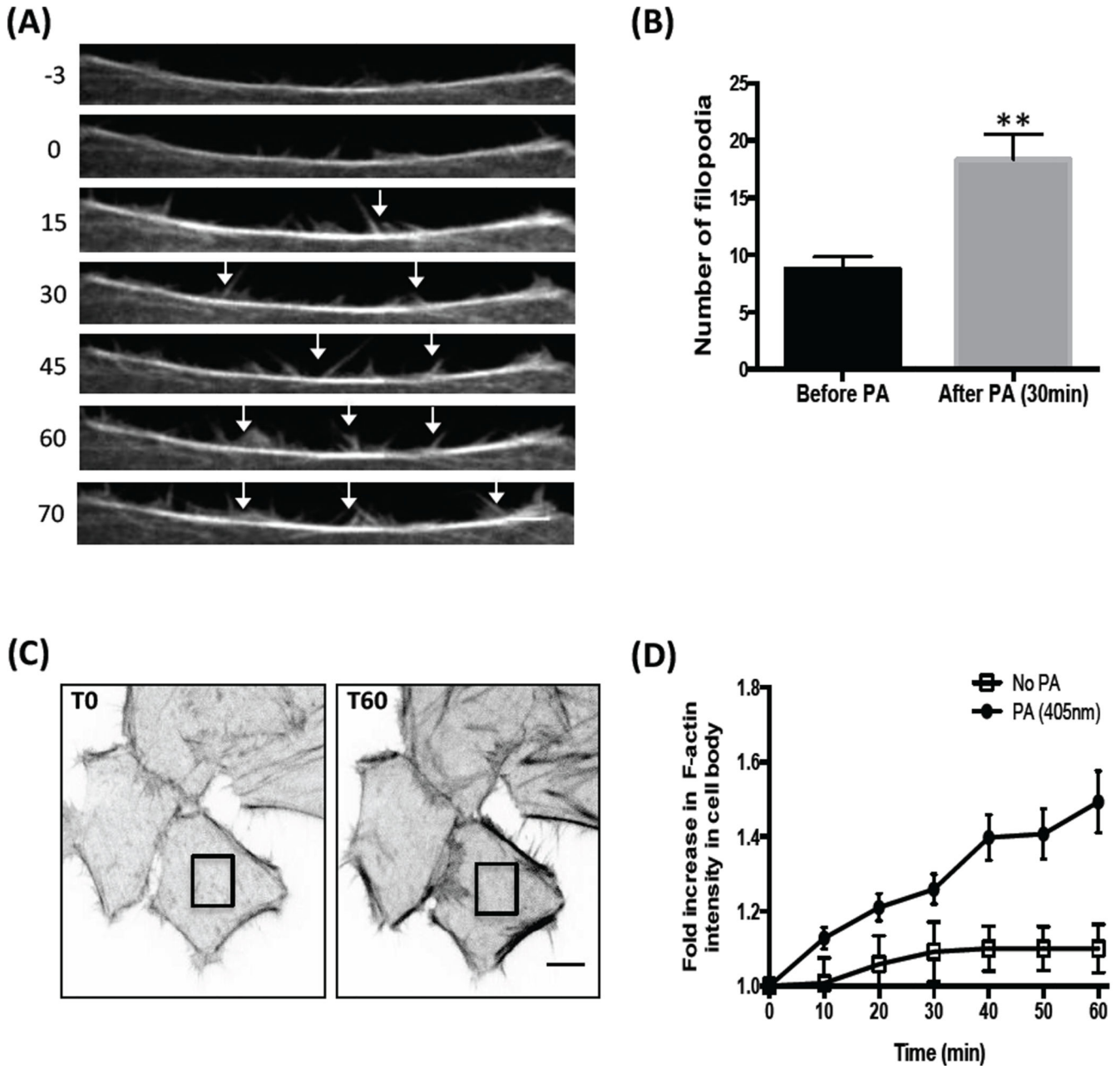
Figure 3.
(A) Example of a cell edge taken from a time-lapse movie showing the formation of multiple transient filopodia (arrows) following repeated photo-activation at 405nm. Time shown in minutes, 0 indicates start of photo-activation. Bar, 10μm. **(B)** Quantification of filopodia before and 30 minutes post-activation (n=10 cells). Error bars indicate s.e.m. (Student's t-test, p<0.05) **(C)** PA-DAD activation stimulates an increase in F-Tractin intensity not only along SFs but also in the cell body, as illustrated by images taken just before and 60 minutes after photoactivation at 405nm. The boxed area within the cell illustrates the type of region used for quantification. Bar, 10μm. **(D)** Quantification of the increase in F-Tractin intensity in the cell body after activation of PA-DAD was done by

marking a box inside the cell in an area devoid of SFs and measuring total intensity over time (n= 12 cells for No PA and 15 cells for PA at 405nm). Error bars indicate s.e.m.
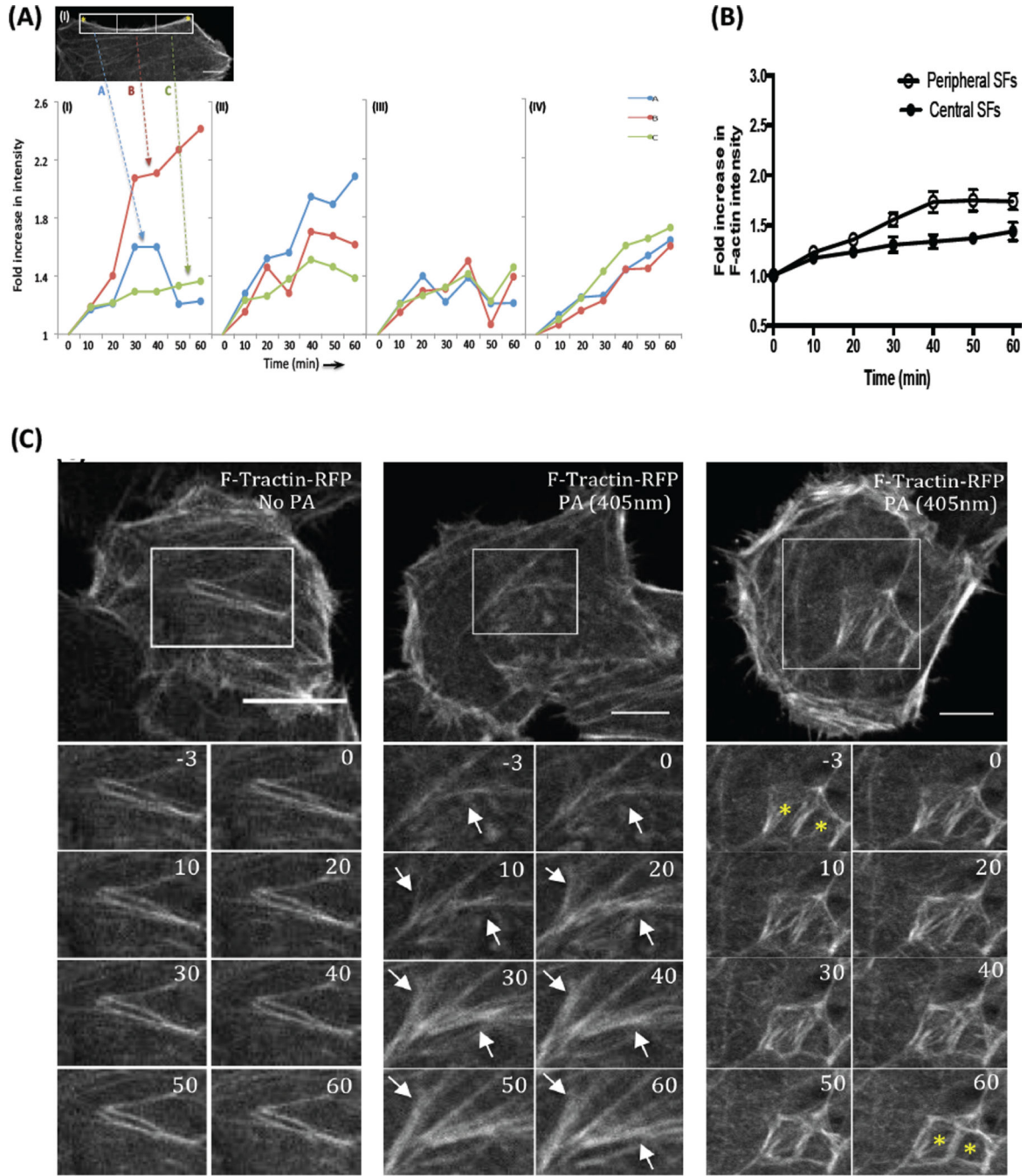
Figure 4. F-actin polymerization along existing SF following PA-DAD activation
(**A**) Actin polymerization occurs all along SFs and is not necessarily initiated at FAs.
Examples from four different peripheral SFs (I, II, III and IV) are shown here. Each SF was
segmented into three equal parts A, B and C and change in fluorescent intensity of each
segment was followed over time, as illustrated for SF-I. Yellow asterisks indicate points of
anchorage of SFs at FAs in segment A and C. (**B**) Comparison of central and peripheral SFs
(n=11 and 13 respectively) after photo-activation, showing increase in intensity of both
kinds of SFs. Error bars represent s.e.m. (**C**) PA-DAD activation leads to actin

polymerization within existing central SFs in cells, with cases of branching, divergence (white arrows) and coalescence (yellow asterisks) of SFs observed. Note that in conditions of no photo-activation (No PA), central SFs do not change during the course of imaging. Time indicated in minutes, 0 represents start of photo-activation. Bar, 10μm.
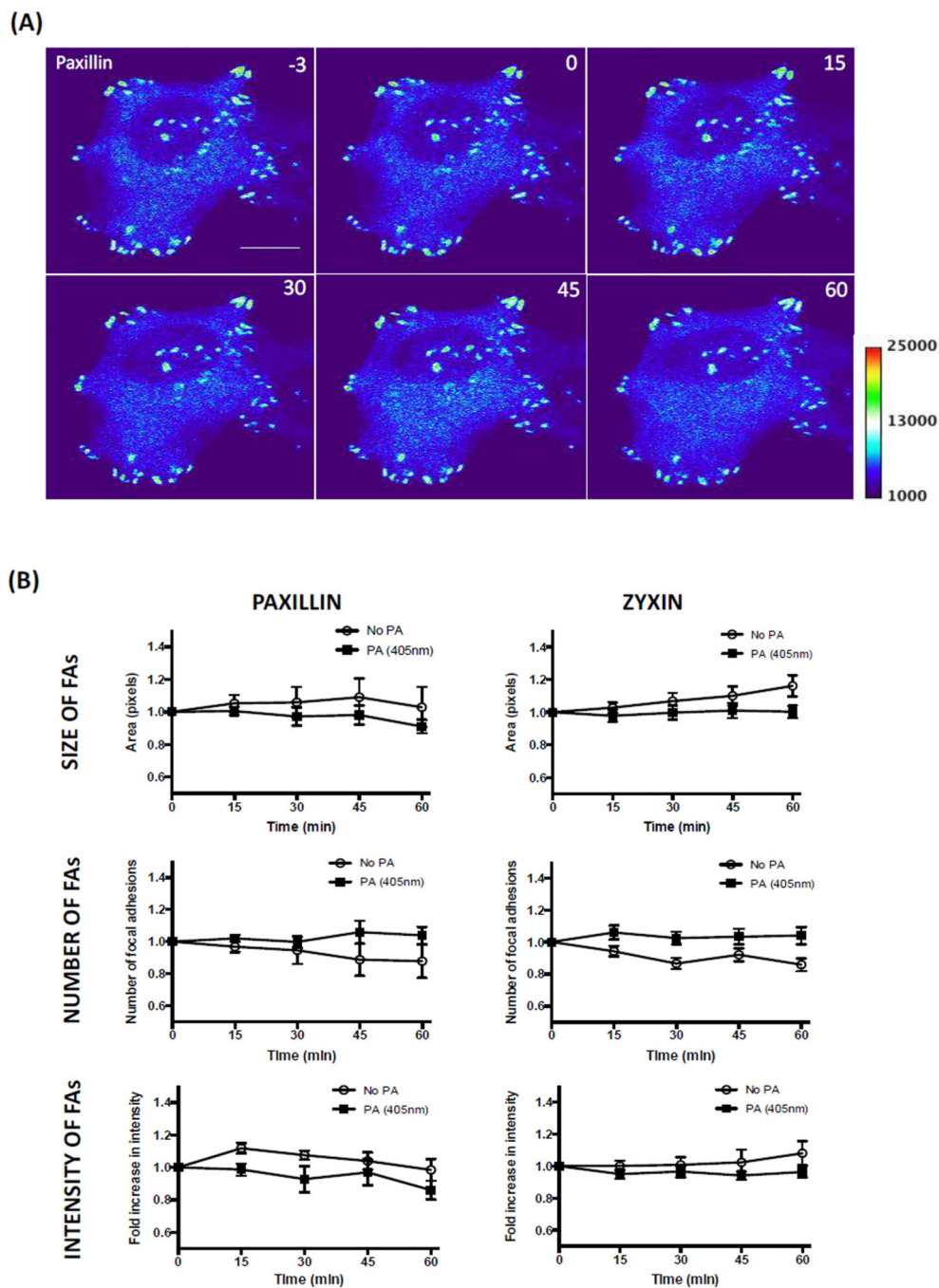
Figure 5. Photo-activation of PA-DAD does not lead to an increase in the size, number or intensity of FA

(**A**) Representative images from a time-lapse movie of paxillin-labeled focal adhesions during repeated photo-activation of PA-DAD; time indicated in minutes, 0 represents start of photo-activation. Bar, 10μm. (**B**) Quantification of size, number and fluorescent intensity of paxillin or zyxin-labeled focal adhesions from HeLa cells co-transfected with mVenus-PA-DAD and the respective focal adhesion marker tagged with mCherry (n>500 FAs from 7–9

cells for No PA and repeated PA conditions for both paxillin and zyxin). Error bars represent s.e.m.
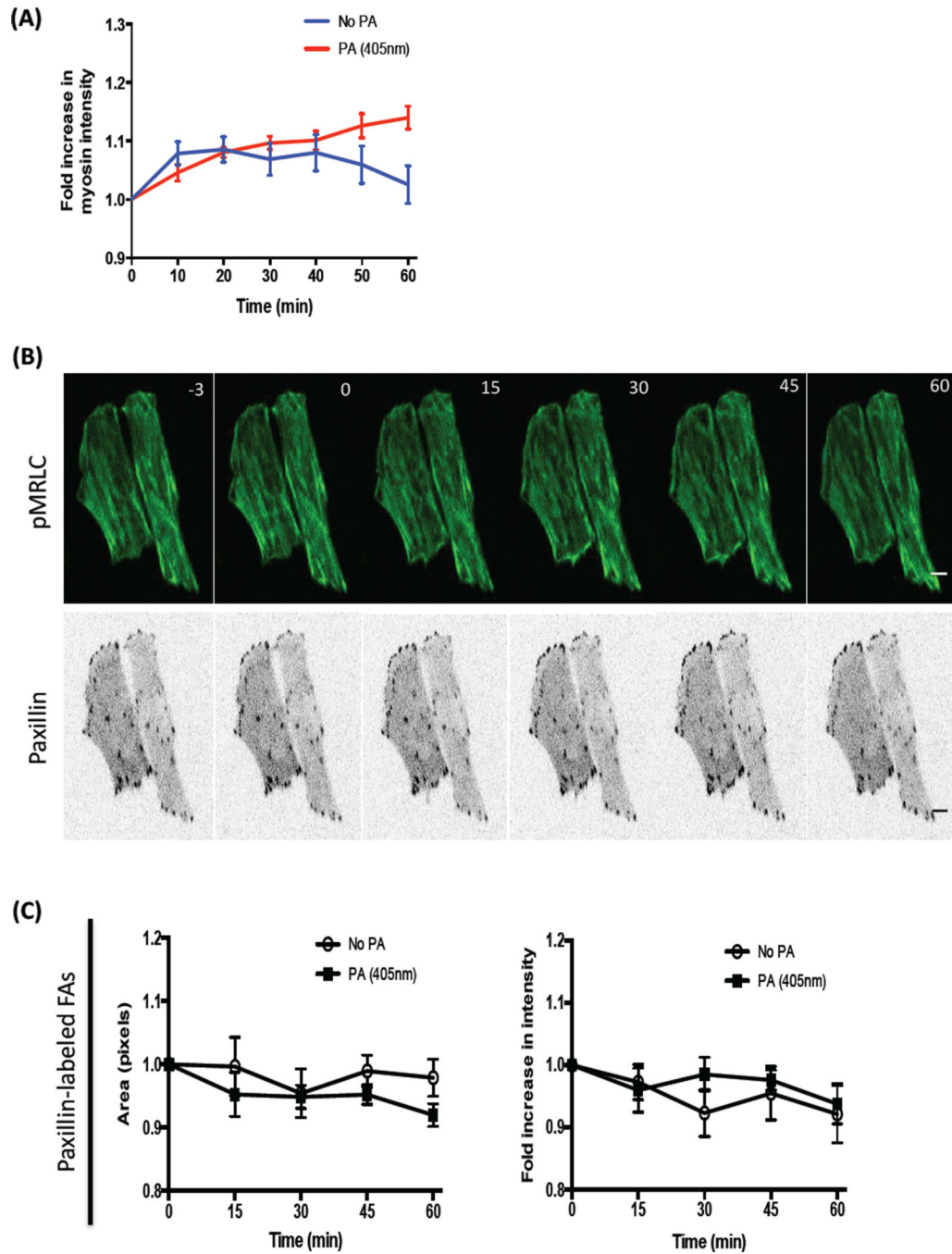
Figure 6. Myosin recruitment into SFs is not significantly increased following PA-DAD photo-activation

(**A**) Quantification of GFP-tagged Myosin Regulatory Light Chain levels in SF following photoactivation of PA-DAD. (n=11 cells for No PA, 12 cells for PA at 405nm). Error bars represent s.e.m. (**B**) Representative images from a time-lapse movie of HeLa cells expressing phosphomimetic MRLC, mCherry-Paxillin and eBFP-PA-DAD, subjected to repeated photo-activation. Note that there is no significant change in either pMRLC or paxillin-labeled FAs. Both cells shown here express eBFP-PA-DAD. Time indicated in

minutes, 0 represents start of photo-activation. Bar, 5μm. **(C)** Quantification of FA size and intensity in HeLa cells expressing a constitutively active form of myosin (phosphomimetic MRLC), mCherry-Paxillin and eBFP-PA-DAD, subjected to repeated photo-activation (n>500 FAs from 7 cells for no PA and with PA at 405nm). Error bars represent s.e.m.